HOKKAIDO UNIVERSITY

Title	Periodontal tissue engineering by nano beta-tricalcium phosphate scaffold and fibroblast growth factor-2 in one-wall infrabony defects of dogs
Author(s)	Ogawa, Kosuke; Miyaji, Hirofumi; Kato, Akihito; Kosen, Yuta; Momose, Takehito; Yoshida, Takashi; Nishida, Erika; Miyata, Saori; Murakami, Shusuke; Takita, Hiroko; Fugetsu, Bunshi; Sugaya, Tsutomu; Kawanami, Masamitsu
Citation	Journal of Periodontal Research, 51(6), 758-767 https://doi.org/10.1111/jre.12352
Issue Date	2016-12
Doc URL	http://hdl.handle.net/2115/68175
Rights	This is the peer reviewed version of the following article: [Periodontal tissue engineering by nano beta-tricalcium phosphate scaffold and fibroblast growth factor-2 in one-wall infrabony defects of dogs], which has been published in final form at [https://doi.org/10.1111/jre.12352]. This article may be used for non-commercial purposes in accordance with Wiley Terms and Conditions for Self-Archiving.
Type	article (author version)
File Information	2016 Ogawa J Periodont Res.pdf

Instructions for use

Hokkaido University Collection of Scholarly and Academic Papers : HUSCAP

Periodontal tissue engineering by nano beta-TCP scaffold and FGF-2 in 1-wall infrabony defects of dogs

Kosuke OGAWA[1], Hirofumi MIYAJI[1], Akihito KATO[1], Yuta KOSEN[1], Takehito MOMOSE[1], Takashi YOSHIDA[1], Erika NISHIDA[1], Saori MIYATA[1], Shusuke MURAKAMI[1], Hiroko TAKITA[2], Bunshi FUGETSU[3], Tsutomu SUGAYA[1], Masamitsu KAWANAMI[1]

Institutions

1. Department of Periodontology and Endodontology, Hokkaido University Graduate School of Dental Medicine, Sapporo, Japan
2. Support Section for Education and Research, Hokkaido University Graduate School of Dental Medicine, Sapporo, Japan
3. Nano-Agri Lab, Policy Alternatives Research Institute, The University of Tokyo, Tokyo, Japan

Running title

Periodontal healing by nano β-TCP and FGF-2

Key words

Periodontal tissue engineering, Fibroblast growth factor-2 (FGF-2), β-tricalcium phosphate (β-TCP), Nanoparticle, Biomaterial

Correspondence address

Hirofumi MIYAJI

Department of Periodontology and Endodontology, Hokkaido University Graduate School of Dental Medicine, N13 W7 Kita-ku, Sapporo 060-8586, Japan

Abstract

Background and Objective:

Nanoparticle bioceramics are being investigated for biomedical applications. We fabricated a regenerative scaffold comprising type I collagen and beta-tricalcium phosphate (β-TCP) nanoparticles. Fibroblast growth factor-2 (FGF-2) is a bioeffective signaling molecule that stimulates cell proliferation and wound healing. This study examined the effects on bioactivity from a nano-β-TCP/collagen scaffold loaded with FGF-2, particularly on periodontal tissue wound healing.

Material and Methods:

β-TCP was pulverized into nano-sized particles (84 nm) and was then dispersed. Nano-β-TCP scaffold was prepared by coating the surface of a collagen scaffold with a nano-sized β-TCP dispersion. Scaffolds were characterized using scanning electron microscopy (SEM), compressive testing, cell seeding, and rat subcutaneous implant testing. Then nano-β-TCP scaffold, nano-β-TCP scaffold loaded with FGF-2, and non-coated collagen scaffold were implanted into a dog 1-wall infrabony defect model. Histological observations were made at 10 d and 4 wk post-surgery.

Results:

Results of SEM observation show that TCP nanoparticles were attached to collagen fibers. Nano-β-TCP scaffold showed higher compressive strength and cytocompatibility than non-coated collagen scaffold. Rat subcutaneous implant tests showed that DNA contents of infiltrating cells in the nano-β-TCP scaffold and FGF2-loaded scaffold were each approximately 2.8-fold and 3.7-fold greater than the collagen scaffold. Histological samples from the periodontal defect model showed about five-fold greater periodontal tissue repair following implantation of the nano-β-TCP scaffold loaded with FGF-2 rather than the collagen scaffold.

Conclusion:

The β-TCP nanoparticle coating strongly improved the collagen scaffold bioactivity. Nano-β-TCP scaffolds with FGF-2 are anticipated for use in periodontal tissue engineering.

Introduction

Periodontal tissue engineering has been investigated extensively for repairing lost periodontal attachment and alveolar bone by severe periodontitis (1). Three major elements are crucial for periodontal tissue engineering strategies: cells, signaling molecules, and natural or artificial scaffolds. Scaffolds play an important role in growth factor storage and space maintenance for tissue reconstruction (2) and in stem cell proliferation and differentiation. Reportedly, modification of the regenerative scaffold surface produces various biological properties, thereby increasing scaffold bioactivity (3). Particularly, modification of a scaffold using nano-sized materials increases the surface area and scaffold roughness (4), improves compressive strength (5), and enhances protein adsorption (6). *In vivo* reports have described that nano-modified scaffolds have superior biological properties including biodegradation (7), cell ingrowth (8), and osteoconductivity (9).

In bone tissue engineering approaches, bioceramic materials such as calcium phosphate (10), hydroxyapatite (HA) (11), bioactive glass (12), and composites (13) have been applied as scaffolds. Actually, nano-sized bioceramics can strongly affect the biocompatibility of scaffolds. Okada et al. reported that fibroblast adhesion and proliferation to the HA surface of nanoparticles with 50–100 nm diameter were promoted significantly when compared with HA having a flat surface (14). Furthermore, biphasic calcium phosphate (BCP) ceramics with nanometer or submicrometer structures have better protein adsorption and osteoconductivity than conventional BCP ceramics (15). Recently, we fabricated a collagen scaffold coated with an aqueous dispersion of nanosized particles of beta-tricalcium phosphate (β-TCP). This scaffold exhibited a nanostructural surface consisting of TCP nanoparticles and promoted bone augmentation in rat cranial bone (16). Therefore, the TCP nanoparticle/collagen scaffold might be useful for periodontal tissue engineering.

Fibroblast growth factor-2 (FGF-2) stimulates cell viability associated with wound healing, such as cell proliferation, migration, and differentiation (17). In addition, FGF-2 promotes the growth of periodontal ligament cells and osteogenic cells such as osteoblasts and bone marrow stromal cells (18, 19). Many studies have demonstrated that a regenerative scaffold combined with FGF-2 facilitated rapid tissue ingrowth in the inner space and stimulated bone formation effects in a rat model (16, 20). Based on these results, we hypothesized that scaffolds containing β-TCP nanoparticles and FGF-2 promote periodontal healing through multiple mechanisms. Such a study has not yet been reported in the literature. Accordingly, the aim of this study was to examine the biological effects of nano-β-TCP scaffold loaded with FGF-2 on periodontal tissue healing. Scaffolds were implanted into rat subcutaneous tissue and dog 1-wall infrabony periodontal defects as preclinical tests to assess the biological effects of nanomodification and FGF-2 application.

Materials and Methods

Fabrication and characterization of nano-β-TCP scaffold

Nano-β-TCP dispersion (1 wt%) was prepared as described previously [16, 21]. β-TCP (average particle size: 2.3 μm; Tomita Pharmaceutical Co. Ltd., Naruto, Japan) was pulverized into nanosized particles using a pulverizer (Nanomizer Inc., Yokohama, Japan). The TCP nanoparticles were then dispersed along with the surfactant sodium cholate (0.2 wt%) in 1-methyl-2-pyrrolidone (Wako Pure Chemical Industries Ltd., Osaka, Japan). The mean particle size of TCP was found to be 84.4 nm from particle size distribution analysis (LB-550; Horiba Ltd., Kyoto, Japan).

Collagen scaffold (Terudermis®; 6 × 6 × 3 mm^3, average porosity 97.3%; Olympus Terumo Biomaterials Corp., Tokyo, Japan) was immersed in a nano-β-TCP dispersion. After rinsing in ethanol and air-drying, the nano-β-TCP scaffold was obtained (Fig. 1A).

Scaffolds were characterized using a scanning electron microscope (SEM) (S-4000; Hitachi Ltd., Tokyo, Japan) with accelerating voltage of 10 kV. Compression tests were conducted using a universal testing machine (EZ-S; Shimadzu Corp., Kyoto, Japan). The cross-head loading speed was set to 0.5 mm/min. Porosity of the scaffold was calculated using the following equation: porosity = $100 \times (1-\rho 1/\rho 2)$, where $\rho 1$ = bulk density and $\rho 2$ = theoretical density of the scaffold.

Cytocompatibility test

Mouse osteoblastic MC3T3-E1 cells (1×10^4; RIKEN BioResource Center, Tsukuba, Japan) were seeded on scaffolds and cultured in humidified 5% CO_2 at 37°C, using minimum essential medium (MEM) (alpha-GlutaMAX™-I; Thermo Fisher Scientific Inc., Waltham, MA) supplemented with 10% fetal bovine serum (FBS) (Qualified; Thermo Fisher Scientific Inc.) and 1% antibiotics (penicillin/streptomycin; Thermo Fisher Scientific Inc.). Cell viability was assessed after 1 and 3 days of culture using a cell counting kit-8 (CCK-8; Dojindo Laboratories, Mashiki, Japan), in accordance with the manufacturer's instructions.

After 1 day of culture, some samples were fixed in 2.5% glutaraldehyde in 0.1 M sodium cacodylate buffer (pH 7.4) for 30 min, and were rinsed in cacodylate buffer solution. Samples were then dehydrated in increasing concentrations of ethanol. Following critical point drying, samples were analyzed by SEM.

FGF-2 implant preparation and FGF-2 adsorption assay

FGF-2 (KCB-1D; Kaken Pharmaceutical Co. Ltd., Tokyo, Japan) was diluted with distilled water (Otsuka distilled water; Otsuka Pharmaceutical Co. Ltd., Tokyo, Japan) to

produce stock solution of 0.5 μg/μL, as described in a previous report (16, 20). In the FGF-2-loading group, nano-β-TCP scaffolds were injected with 100 μL of FGF-2 solution (loading dose; 50 μg) under vacuum. In the other groups, each sample received distilled water alone.

To detect immobilized FGF-2 on the scaffold, an FGF-2 loaded scaffold was placed in 1 ml of distilled water. After stirring well, the protein content of the supernatant was assessed using a total protein kit (Micro Lowry, Peterson's Modification; Sigma-Aldrich Corp., St. Louis, MO) in accordance with the manufacturer's instructions. As a control, protein content of 100 μL of FGF-2 stock solution was also measured.

Rat subcutaneous test

The experimental protocols followed the institutional animal use and care regulations of Hokkaido University (Approval number 10-42; Animal Research Committee of Hokkaido University). Eight 10-week-old male Wistar rats weighing 190–210 g were given general anesthesia by intraperitoneal injections of 0.6 mL/kg sodium pentobarbital (Somnopenthyl; Kyoritsu Seiyaku Corp., Tokyo, Japan) and a local injection of 2% lidocaine hydrochloride with 1:80,000 epinephrine (Xylocaine Cartridge for Dental Use; Dentsply Sankin K.K., Tokyo, Japan).

After a skin incision was made, nano-β-TCP scaffold or FGF-2-loaded nano-β-TCP scaffold was implanted into the subcutaneous tissue of the back of each rat. In addition, a collagen scaffold was implanted as control. Skin flaps were sutured (Softretch 4-0; GC, Tokyo, Japan) and tetracycline hydrochloride ointment (Achromycin Ointment; Pola Pharma Inc., Tokyo, Japan) was applied to the wound.

Rats were euthanized using an overdose of sodium pentobarbital (2.0 mL/kg) at 10 days post-surgery. Several specimens extracted from the wound were freeze-dried. Following pulverization, 0.5 mL of 2 M NaCl and 0.05 M phosphate buffer (pH 7.4) were added to each scaffold. After centrifugation, the DNA content of each scaffold was examined using a DNA quantification kit (Primary Cell Co. Ltd., Sapporo, Japan) and a fluorescence spectrophotometer at the respective excitation and emission wavelengths of 356 nm and 458 nm.

Several samples were collected for histological observation. Tissue blocks, including the surrounding soft tissues, were fixed in 10% buffered formalin, embedded in paraffin wax, and cut into 5-μm sections. Sections were stained with hematoxylin–eosin (HE) and observed histologically by light microscopy.

Application of nano β-TCP scaffold to periodontal defect model

Four healthy female beagle dogs, aged 10 months and weighing approximately 9–10 kg,

were used in this experiment. Experimental protocols conformed to the institutional animal use and care regulations of Hokkaido University (Approval number 8-255). Surgical procedures were performed under general anesthesia with medetomidine hydrochloride (0.1 ml/kg, Domitor; Nippon Zenyaku Kogyo Co. Ltd., Koriyama, Japan) and butorphanol tartrate (0.1 ml/kg, Vetorphale; Meiji Seika Pharma Co. Ltd., Tokyo, Japan), and under local anesthesia with lidocaine hydrochloride. The mandibular first and third premolars were extracted before experimental surgery. The extraction sites were allowed to heal for eight weeks.

Following reflection of the buccal and lingual muco-gingival flaps with partial thickness, periosteum was removed from the alveolar bone. One-wall infrabony defects (5 mm depth; 3 mm width) were surgically created in the mesial and distal aspect of the mandibular second premolars, and in the mesial aspect of the mandibular fourth premolars. The root surface facing the defect was planed to remove cementum. Reference notches indicating the cement–enamel junction and bottom of the defect were prepared on the root surface (Fig. 1B). The denuded root surface was demineralized using 24% EDTA (pH 7.0) for 3 min and washed with saline. Subsequently, defects were assigned randomly to the three groups and filled with FGF-2 loaded nano-β-TCP, nano-β-TCP, or collagen scaffold (Fig. 1C). The flap was repositioned and sutured securely (Surgilon; Covidien, Tokyo, Japan) (Fig. 1D). Animals received ampicillin sodium (300 mg/kg, Viccillin; Meiji Seika Pharma Co. Ltd., Tokyo, Japan) daily for three days and a plaque control regimen with 0.5% chlorhexidine (Hibitane; Dainippon Sumitomo Pharma, Tokyo, Japan) twice weekly for the entire duration of the experiment. Radiographic images of periodontal defects were taken immediately following surgery and at 4 weeks after scaffold implantation.

Histological observations and measurements of periodontal healing

Animals were euthanized at 10 days and 4 weeks post-surgery using an overdose of sodium pentobarbital (0.5 ml/kg), following general anesthesia with medetomidine hydrochloride (0.1 ml/kg) and butorphanol tartrate (0.1 ml/kg). Tissue blocks, including teeth, bone, and soft tissue, were fixed in 10% buffered formalin, decalcified in 10% formic-citric acid and embedded along the mesial–distal plane in paraffin wax. Sections (6 μm) were serially prepared and stained with HE and Masson's trichrome stains.

Three HE-stained sections were taken. One was approximately from the center of the root. The other two were 180 μm from either side of the center. The following five histomorphometric measurements (Fig. 2) were taken for each stained section using software (Image J 1.41; National Institutes of Health, Bethesda, MD).

1. Bone height: distance between the apical notch and the coronal extension of newly formed alveolar bone along the root surface

2. Bone area: newly formed alveolar bone in the defect area
3. Periodontal ligament-like tissue: length of fibrous tissue between newly formed cementum-like tissue and alveolar bone
4. Cementum-like tissue: distance between the apical notch and coronal extension of newly formed cementum-like tissue on the root surface
5. Gingival recession: distance between the cement–enamel junction and the gingival margin

Statistical analysis

Means and standard deviations were calculated for each parameter. Differences between groups were analyzed using Student's *t*-test for structural parameters, cell proliferation, and protein assay, with Scheffé's test for DNA content and parameters related to periodontal wound healing. *P* values of < 0.05 were regarded as statistically significant. All statistical procedures were performed using software (SPSS, IBM SPSS 11.0; IBM Japan Ltd., Tokyo, Japan).

Results

Characterization of nano-β-TCP scaffold

Based on SEM observation, nano-sized β-TCP particles attached to the surface of collagen scaffold struts. The inner spaces of collagen scaffolds were not filled with β-TCP (Figs. 3A–3D). Porosity was calculated as > 95% (Table 1). Compressive strength of the nano-β-TCP scaffold was approximately 1.2-fold greater than that of the collagen scaffold (Table 1).

Cytocompatibility of nano-β-TCP scaffold

SEM observation revealed that osteoblastic MC3T3-E1 attached to the nano-β-TCP scaffold. Moreover, cell spreading and cell process elongation was frequently observed (Fig. 3E). On CCK-8 assay, E1 cells proliferated significantly on the nano-β-TCP scaffold when compared with the collagen scaffold (Fig. 3F).

Rat subcutaneous test

Samples showed that a few inflammatory cells were present in connective tissue near the implanted scaffolds. The collagen scaffold appeared to be markedly compressed and unable to maintain the cell-invading and regenerative inner space. Consequently, cell and tissue ingrowth were rarely observed in the collagen scaffold (Figs. 4A, 4B). In contrast, ingrowth of fibroblastic cells and blood vessels was observed frequently in peripheral areas of implanted nano-β-TCP scaffold. In addition, macrophage-like giant cells associated with resorption of materials were frequently observed (Figs. 4C, 4D). In the FGF-2-loading group, cell ingrowth

and angiogenesis were demonstrated consistently (Figs. 4E, 4F). DNA contents in the FGF-2-loaded nano-β-TCP scaffold and the unloaded nano-β-TCP scaffold were significantly greater than in the collagen scaffold, with FGF-2 application significantly stimulating DNA levels (Fig. 4G). Protein assay revealed that about 90% of the total FGF-2 was retained on the nano-β-TCP scaffold (Fig. 4H).

Clinical observations of periodontal healing

The postoperative healing process appeared to be favorable in all dogs. At 4 weeks, macroscopic findings exhibited evidence of gingival recession in the collagen scaffold group. Bone defects treated with FGF-2 showed increased radiopacity (Fig. 5).

Histological observations of periodontal healing

At 10 days, gingival connective tissue and epithelium in the collagen scaffold receiving group occupied about half the area of the defect (Fig. 6A). In contrast, periodontal defect was mostly occupied by residual scaffold in the nano-β-TCP scaffold receiving group (Figs. 6B, 6C). In addition, the FGF2 receiving group clearly showed ingrowth of fibroblastic cells and blood vessel-like tissue in the scaffold (Fig. 6D). Particularly, formation of woven bone was promoted when compared with collagen scaffold and nano-β-TCP scaffold receiving groups (Fig. 6E).

At 4 weeks, with FGF-2-loaded scaffold implantation, a marked degree of new bone formation was observed (Fig. 7A). New bone was composed of narrow trabeculae including osteoblasts and osteocyte-like cells (Fig. 7B), occupying more than half of the defect space. In the coronal portion, fibrous connective tissue faced the instrumented root surfaces. Epithelial downgrowth was rarely observed (Fig. 7C). Acellular cementum-like tissue that was continuous from the pre-existing root cementum was also widely observed on the root dentin surface (Fig. 7D). Furthermore, periodontal ligament-like tissue was established between new bone and cementum-like tissue (Fig. 7D). Masson's staining clearly showed rich connective tissue, but a fiber structure resembling Sharpey's fibers was observed slightly in the newly formed fibrous tissue (Fig. 7E).

Although periodontal tissue repair was observed with the nano-β-TCP scaffold, the amount of reconstructed tissue was lower than in the FGF-2-treated group. Periodontal ligament-like tissue partly formed on the apical portion of the root surface. In the coronal portion, gingival connective tissue was well developed (Figs. 8A, 8C). In the collagen scaffold-treated group, some tissue formation, including cementum-like tissue and alveolar bone, was observed around the apical notch. In addition, gingival recession was seen frequently. The instrumented root was exposed together with dental plaque infection (Figs. 8B, 8D).

No specimen showed any residual material, including β-TCP and collagen. We observed

no aberrant healing such as root resorption and ankylosis in any group.

Histomorphometric analysis of periodontal healing

The degree of periodontal tissue healing in 1-wall infrabony defects is shown in Fig. 9. Significant bone formation was observed when the nano-β-TCP scaffold was used, as compared to the control group. The FGF2-loaded group showed the most active bone formation among the three groups. The mean values of bone height and area in the FGF-2-treated group were approximately 3.3-fold and 6.2-fold greater than in the collagen scaffold group, respectively (Figs. 9A, 9B). Formation of cementum-like tissue and periodontal ligament-like tissue in the FGF-2-treated group, increased significantly when compared with samples treated with collagen scaffold. Mean values for cementum-like tissue and periodontal ligament-like tissue in the FGF-2 group were approximately 5.1-fold and 5.5-fold greater than in the collagen scaffold group, respectively (Figs. 9C, 9D). Significant gingival recession was observed in the collagen scaffold group (Fig. 9E).

Discussion

Application of β-TCP nanoparticles to the collagen scaffold distinctly improved *in vitro* cell proliferation and *in vivo* tissue ingrowth into the scaffold when compared with the unmodified collagen scaffold. β-TCP is widely known to possess good osteoconductivity (22, 23). However, our examination revealed that nano-sized TCP modification improved cell ingrowth in rat subcutaneous non-osteogenic tissue. Ordinarily, the surface morphology of the interface between cells and biomaterials strongly affects cell behavior. Particularly nano-modification of biomaterials might increase the surface area and signaling molecule adsorption (4, 8, 24). Woo et al. (25) reported that a synthetic nano-fibrous scaffold, mimicking the structure of natural collagen fibers, enhanced the adsorption of proteins such as fibronectin and osteoblastic cell attachment, thereby suggesting a more favorable microenvironment/nanoenvironment for cells on the scaffold. Furthermore, the nano-HA/ poly L-lactic acid composite scaffold showed good protein adsorption in comparison with micron-HA (26). Accordingly, nanomaterials would be beneficial in tissue healing because the regenerative space retained biological factors involved in growth, differentiation, and nutrition, thereby promoting cell activity and tissue healing. Results suggest that nanostructures using β-TCP nanoparticles provided novel biological properties for collagen scaffolds, stimulating cell invasion on subcutaneous assessment in rats. Furthermore, combination with FGF-2 enhanced cell ingrowth markedly, thereby suggesting that biological responses were up-regulated by FGF-2 immobilized on the scaffold in combination with the nanomorphological effects *in vivo*. Many investigators have reported that FGF-2 promotes proliferation and migration of cell and

repopulation of blood vessels. As a result, FGF-2 was able to accelerate tissue healing after application (27–29). The up-regulation of cell and tissue ingrowth is beneficial for tissue engineering in various tissues and organs.

The compressive strength of the collagen scaffold was reinforced by nanomodification using β-TCP nanoparticles. For periodontal tissue engineering, the scaffold requires sufficient mechanical strength. However, in many cases, higher mechanical strength of scaffold engenders lower porosity, which is unfavorable for cell and tissue ingrowth and degradation (30, 31). Actually, SEM images of nano-β-TCP scaffold showed that nanoparticles of β-TCP did not fill the inner space of the collagen sponge foam, into which regenerative cells were able to infiltrate. Nonetheless, the mechanical strength of the scaffold was significantly higher than that of the untreated collagen scaffold. Recent reports describe that application of nano-carbon materials can further enhance the mechanical strength of collagen sponge scaffolds (4, 5). Kanayama et al. reported that graphene oxide (GO) coating improves the mechanical strength of collagen scaffolds because of the attractive interactions via van der Waals forces between GO substrates at nanoscale distances (5). We speculate that nano-sized β-TCP modification also produces attractive interactions, enhancing physical reinforcement of the collagen scaffold, and thereby providing important benefits as a tissue engineering substrate.

Nano-β-TCP scaffold in the FGF-2-loaded group significantly promoted the repair of periodontal tissues, including bone and cementum-like tissue, while suppressing the gingival recession associated with epithelial downgrowth in the dog 1-wall periodontal defect model. This promotion suggests that the nano-β-TCP scaffold has positive effects on osteoblastic and fibroblastic cell responses, in addition to improving mechanical strength. Based on rat subcutaneous experiments and histological specimens of early periodontal healing, nano-β-TCP scaffold with FGF-2 conceivably guided cells of various types related to periodontal stem cells to the periodontal defect from surrounding tissue. Subsequently, production of extracellular matrix can be expected to occur in the scaffold, thereby suggesting that early regenerative tissue accumulation preceded epithelial downgrowth.

However, periodontal remodeling, i.e., self-reorganization, is extremely difficult to control completely. For example, bone morphogenetic protein (BMP) strongly promotes bone augmentation, but regeneration of the periodontal ligament is rarely observed, and ankylosis is frequently detected (32, 33). In contrast, creation of fibrous tissue such as periodontal membrane and a lack of ankylosis were visible in this study. When bone induction occurred with β-TCP application, implanted β-TCP was resorbed by phagocytosis, resulting in Ca-P ion release (34, 35). These bone inductive elements stimulated the expression of osseous markers in osteoblastic cells, stimulated alkaline phosphatase activity, and adjusted the *in vivo* environment for bone generation (36). In this examination, β-TCP was pulverized into nanoparticles. The

collagen scaffold contained a low volume of β-TCP (1 wt%). Nano-ceramics exhibit high biodegradability when implanted in the body (16). Therefore, TCP nanoparticles appeared to be well-degraded before bone induction and appeared to possess mild effects on osteoconductivity. In actuality, FGF-2 also regulated the proliferation of osteogenic cells such as osteoblasts and bone marrow stromal cells (37, 38). In addition, Lee et al. demonstrated that FGF2 promotes the proliferation of human periodontal ligament stem cells *in vitro* (39). Therefore, we surmised that combination therapy using the nano-β-TCP scaffold and FGF-2 would enable self-assembly for periodontal regenerative tissues, thereby preventing ankylosis. Nano-TCP scaffold therapy is simple and inexpensive when compared with complex methods such as stem cell therapy. We expect that scaffolds using TCP nanoparticles and FGF-2 will be widely used for clinical trials.

The biocompatibility and biosafety of nanomaterials are often discussed for clinical applications. The particle size of nanomaterials plays a major role in cyto-compatibility and tissue-compatibility. Ding et al. reported that intravenous injection of nano-sized HA caused vacuolar degeneration of the nephric tubule epithelium (40). Moreover, oral gavage examination of mice indicated that copper nanoparticles (23.5 nm) are more toxic than microparticles (17 μm) (41). Non-absorbable nanomaterials also remained in cell lysosomes after phagocytosis as a long-term residue (42). However, β-TCP is a bioabsorbable material. Results of this study demonstrate its high biocompatibility. Osteoblastic MC3T3-E1 cells showed good proliferation and attachment to the nano-sized β-TCP modified scaffold surface. In addition, rat experiments revealed good ingrowth of fibroblastic cells. Based on the *in vitro* and *in vivo* evidence, we believe that the FGF-2-loaded nano-β-TCP scaffold possesses good biocompatibility.

Conclusion

The present study specifically addressed the effects of nano-β-TCP scaffolds in combination with FGF-2 on periodontal wound healing. Dispersed β-TCP nanoparticles showed good attachment to the surface of collagen scaffolds, resulting in improved mechanical strength and cell proliferation. Results show that FGF-2 strongly stimulated cell ingrowth and periodontal wound healing. Therefore, scaffolds modified with β-TCP nanoparticles and FGF-2 are expected to be useful as bioeffective devices for periodontal tissue engineering.

Acknowledgements

The authors would like to thank Kaken Pharmaceutical Co. Ltd. for providing FGF-2, Olympus Terumo Biomaterials Corp. for providing collagen scaffolds and Tomita Pharmaceutical Co., Ltd. for providing β-TCP. This work was supported by JPSP KAKENHI Grant no. 22791916 and 25463210. The authors report that they have no conflict of interest related to this study.

References

1. Ivanovski S, Vaquette C, Gronthos S, Hutmacher DW, Bartold PM. Multiphasic Scaffolds for Periodontal Tissue Engineering. *J Dent Res* 2014; **12**: 1212-1221.
2. Hunger PM., Donius AE., UG. Wegst UG. Structure–property–processing correlations in freeze-cast composite scaffolds. *Acta Biomater* 2013; **9**: 6338-6348.
3. Recum AF, Shannon CE, Cannon CE, Long KJ, Kooten TG, Meyle J. Surface roughness, porosity, and texture as modifiers of cellular adhesion. *Tissue Eng* 1996; **2**: 241-253.
4. Nishida E, Miyaji H, Takita H et al. Graphene oxide coating facilitates the bioactivity of scaffold material for tissue engineering. *Jpn J Applied Physics* 2014; **53**: 1-7.
5. Kanayama I, Miyaji H, Takita H et al. Comparative study of bioactivity of collagen scaffolds coated with graphene oxide and reduced graphene oxide. *Int J Nanomedicine* 2014; **9**: 3363-3373.
6. Webster TJ, Ergun C, Doremus RH, Siegel RW, Bizios R. Specific proteins mediate enhanced osteoblast adhesion on nanophase ceramics. *J Biomed Mater Res* 2000; **51**: 475-483.
7. Yokoyama A, Gelinsky M, Kawasaki T et al. Biomimetic porous scaffolds with high elasticity made from mineralized collagen – An animal study. *J Biomed Mater Res Part B* 2005; **75**: 464-472.
8. Yang F, Murugan R, Ramakrishna S, Wang X, Ma YX, Wang S. Fabrication of nano-structured porous PLLA scaffold intended for nerve tissue engineering. *Biomaterials* 2004; **25**: 1891-1900.
9. Xu Q, Lu H, Zhang J, Lu G, Deng Z, Mo A. Tissue engineering scaffold material of porous nanohydroxyapatite/polyamide 66. *Int J Nanomedicine* 2010; **5**: 331-335.
10. Zheng H, Bai Y, Shih M-S et al. Effect of a β-TCP collagen composite bone substitute on healing of drilled bone voids in the distal femoral condyle of rabbits. *J Biomed Mater Res Part B* 2014; **102**: 376-383.
11. Yuan H, van Blitterswijk CA, de Groot K, de Bruijin J. Cross-species comparison of ectopic bone formation in biphasic calcium phosphate (BCP) and hydroxyapatite (HA) scaffolds. *Tissue Eng* 2006; **12**: 1607-1615.
12. Dorozhkin SV. Calcium orthophosphate cements for biomedical application. *J Mater Sci* 2008; **43**: 3028-3057.
13. Causa F, Netti PA, Ciapetti G et al. Poly-ϵ-caprolactone / hydroxyapatite composites for bone regeneration: In vitro characterization and human osteoblast response. *J Biomed Mater Res Part A* 2006; **76**: 151-162.

14. Okada S, Nagai A, Oaki Y, Komotori J, Imai H. Control of cellular activity of fibroblasts on size-tuned fibrous hydroxyapatite nanocrystals. *Acta Biomater* 2011; **7**: 1290-1297.
15. Li B, Liao X, Zheng L et al. Effect of nanostructure on osteoinduction of porous biphasic calcium phosphate ceramics. *Acta Biomater* 2011; **8**: 3794-3804.
16. Ibara A, Miyaji H, Fugetsu B et al. Osteoconductivity and Biodegradability of Collagen Scaffold Coated with Nano-β-TCP and Fibroblast Growth Factor 2. *J Nanomater* 2013; **2013**: 1-11.
17. Yun YR, Won JE, Jeon E et al. Fibroblast growth factors: biology, function, and application for tissue regeneration. *J Tissue Eng* 2010; **1**: 1-18.
18. Murakami S, Takayama S, Ikezawa K et al. Regeneration of periodontal tissues by basic fibroblast growth factor. *J Periodontal Res* 1999; **34**: 425-430.
19. Jeong I, Yu HS, Kim MK, Jang JH, Kim HW. FGF2-adsorbed macroporous hydroxyapatite bone granules stimulate in vitro osteoblastic gene expression and differentiation. *J Materials Sci* 2010; **21**: 1335-1342.
20. Yoshida T, Miyaji H, Otani K et al. Bone augmentation using a highly porous PLGA/β-TCP scaffold containing fibroblast growth factor-2. *J Periodontal Res* 2015; **50**: 265-273.
21. Fugetsu B, Han W, Endo N, Kamiya Y, Okuhara T. Disassembling single-walled carbon nanotube bundles by dipole/dipole electrostatic interactions. *Chem Lett* 2005; **34**: 1218-1219.
22. Saito M, Shimizu H, Beppu M, Takagi M. The role of beta-tricalcium phosphate in vascularized periosteum. *J Orthop Sci* 2000; **5**: 275-282.
23. Koepp HE, Schorlemmer S, Kessler S et al. Biocompatibility and osseointegration of β-TCP: Histomorphological and biomechanical studies in a weight-bearing sheep model. *J Biomed Mater Res Part B* 2004; **70**: 209-217.
24. Engel E, Michiardi A, Navarro M, Lacroix D, Planell JA : Nanotechnology in regenerative medicine: The materials side. *Trends Biotechnol* 2008; **26**: 39-47.
25. Woo KM, Chen VJ, Ma PX. Nano-fibrous scaffolding architecture selectively enhances protein adsorption contributing to cell attachment. *J Biomed Mater Res Part A* 2003; **67**: 531-537.
26. Wei G, Ma PX. Structure and properties of nano-hydroxyapatite/polymer composite scaffolds for bone tissue engineering. *Biomaterials* 2004; **25**: 4749-4757.
27. Boilly B, Vercoutter-Edouart AS, Hondermarck H, Nurcombe V, Le Bourhis X. FGF signals for cell proliferation and migration through different pathways. *Cytokine Growth Factor Rev* 2000; **11**: 295-302.

28. Jansen RG, Van Kuppevelt TH, Daamen WF, Kuijpers-Jagtman AM, Von den Hoff JW. FGF-2-loaded collagen scaffolds attract cells and blood vessels in rat oral mucosa. *J Oral Pathol Med* 2009; **38**: 630-638.
29. Park HJ, Lee S, Kang KH et al. Enhanced random skin flap survival by sustained delivery of fibroblast growth factor 2 in rats. *ANZ J Surg* 2013; **83**: 354-358.
30. Bose S, Darsell J, Kintner M, Hosick H, Bandyopadhyay A. Pore size and pore volume effects on alumina and TCP ceramic scaffolds. *Materials Science and Engineering Part C* 2003; **23**: 479-485.
31. Kasten P, Beyen I, Niemeyer P, Luginbuhl R, Bohner M, Richter W. Porosity and pore size of β-tricalcium phosphate scaffold can influence protein production and osteogenic differentiation of human mesenchymal stem cells: an in vitro and in vivo study. *Acta Biomater* 2008; **4**: 1904-1915.
32. King GN, Hughes FJ. Effects of occlusal loading on ankylosis, bone, and cementum formation during bone morphogenetic protein-2-stimulated periodontal regeneration in vivo. *J Periodontol* 1999; **70**: 1125-1135.
33. Miyaji H, Sugaya T, Ibe K, Ishizuka R, Tokunaga K, Kawanami M. Root surface conditioning with bone morphogenetic protein-2 facilitates cementum-like tissue deposition in beagle dogs. *J Periodontal Res* 2010; **45**: 658-663.
34. Nagayama M, Takeuchi H, Doi Y. Comparison of carbonate apatite and beta-tricalcium phosphate (resorbable calcium phosphates) implanted subcutaneously into the back of rats. *Dent Mater J* 2006; **25**: 219-225.
35. Cai S, Xu GH, Yu XZ, Zhang WJ, Xiao ZY, Yao KD. Fabrication and biological characteristics of beta-tricalcium phosphate porous ceramic scaffolds reinforced with calcium phosphate glass. *J Mater Sci Mater Med* 2009; **20**: 351-358.
36. Xia L, Zhang Z, Chen L et al. Proliferation and osteogenic differentiation of human periodontal ligament cells on akermanite and β-TCP bioceramics. *Eur Cell Mater* 2011; **22**: 68-83.
37. Hong KS, Kim EC, Bang SH et al. Bone regeneration by bioactive hybrid membrane containing FGF2 within rat calvarium. *J Biomed Mater Res Part A* 2010; **94**: 1187-1194.
38. Fei Y, Xiao L, Doetschman T, Coffin DJ, Hurley MM. Fibroblast growth factor 2 stimulation of osteoblast differentiation and bone formation is mediated by modulation of the Wnt signaling pathway. *J Biol Chem* 2011; **286**: 40575-40583.
39. Lee JH, Um S, Jang JH, Seo BM. Effects of VEGF and FGF-2 on proliferation and differentiation of human periodontal ligament stem cells. *Cell Tissue Res* 2012; **348**: 475-484.

40. Ding T, Xue Y, Lu H, Huang Z, Sun J. Effect of particle size of hydroxyapatite nanoparticles on its biocompatibility. *IEEE Trans Nanobioscience* 2012; **11**: 336-340.
41. Chen Z, Meng H, Xing G et al. Acute toxicological effects of copper nanoparticles in vivo. *Toxicol Lett* 2006; **163**: 109-120.
42. Wang K, Ruan H, Song H et al. Biocompatibility of graphene oxide. *Nanoscale Res Lett* 2011; **6**: 1-8.

Table 1. Structural parameters of the scaffold (N = 6, mean ± SD)

	Collagen scaffold	Nano-β-TCP scaffold
Weight (mg/mm^3)	0.033 ± 0.002	0.039 ± 0.002*
Compressive strength (MPa)	0.073 ± 0.007	0.088 ± 0.008*
Porosity (%)	97.67 ± 0.13	96.34 ± 0.07*

* Statistically significant difference compared to collagen scaffold.

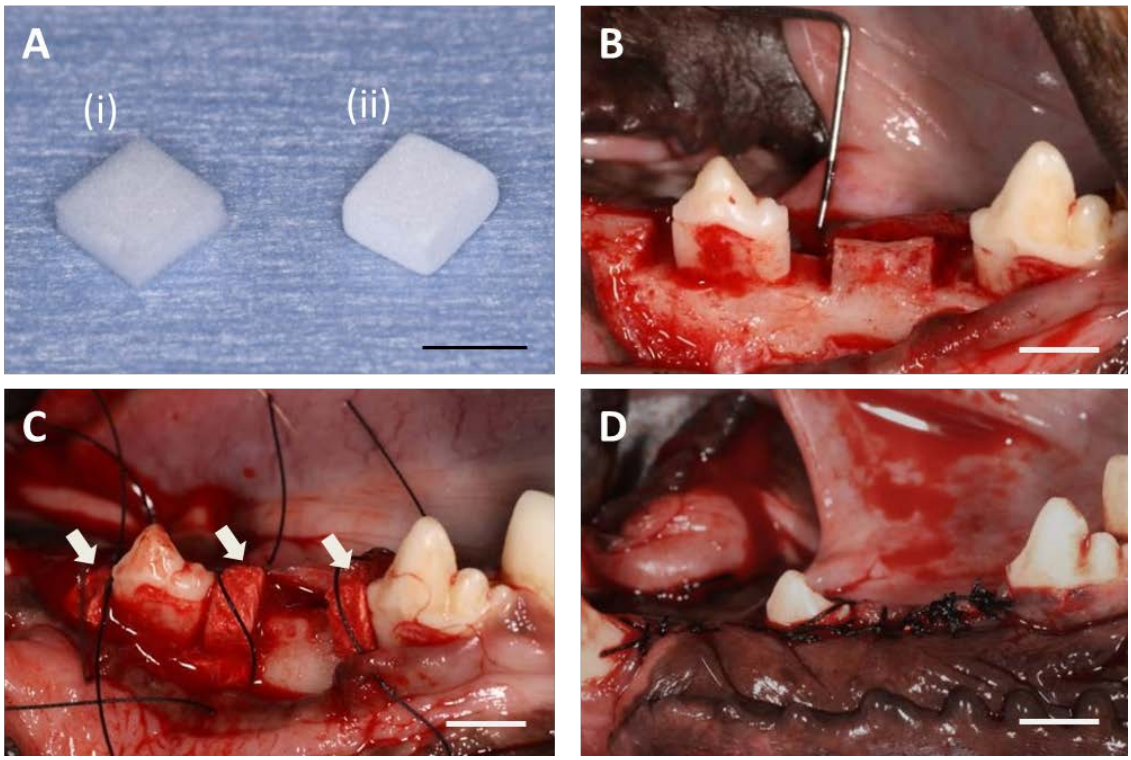

Figure 1

Digital photographs of scaffolds (A) and surgical procedures (B–D). (A) Collagen scaffold (i) and nano-β-TCP scaffold (ii). (B) After the flap was elevated, one-wall infrabony defects were surgically created. (C) Defects were filled with scaffold (arrows). (D) The flap was repositioned and sutured securely. Scale bars represent 5 mm.

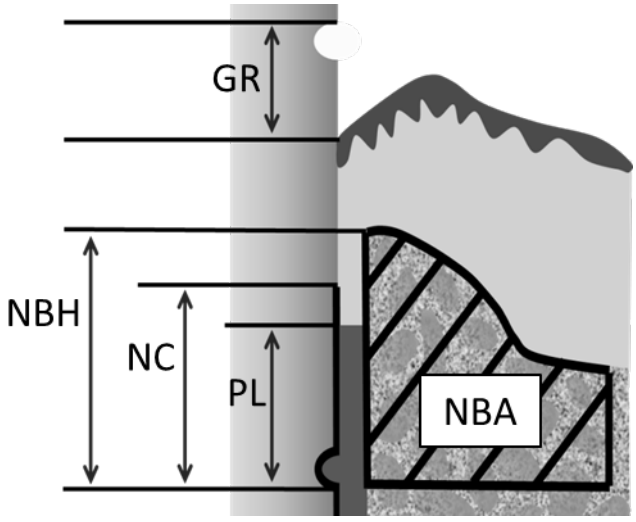

Figure 2

Schematic drawing of histomorphometric analysis of periodontal wound healing: NBH, new bone height; NBA, new bone area; PL, new periodontal ligament-like tissue; NC, new cementum-like tissue; GR, gingival recession.

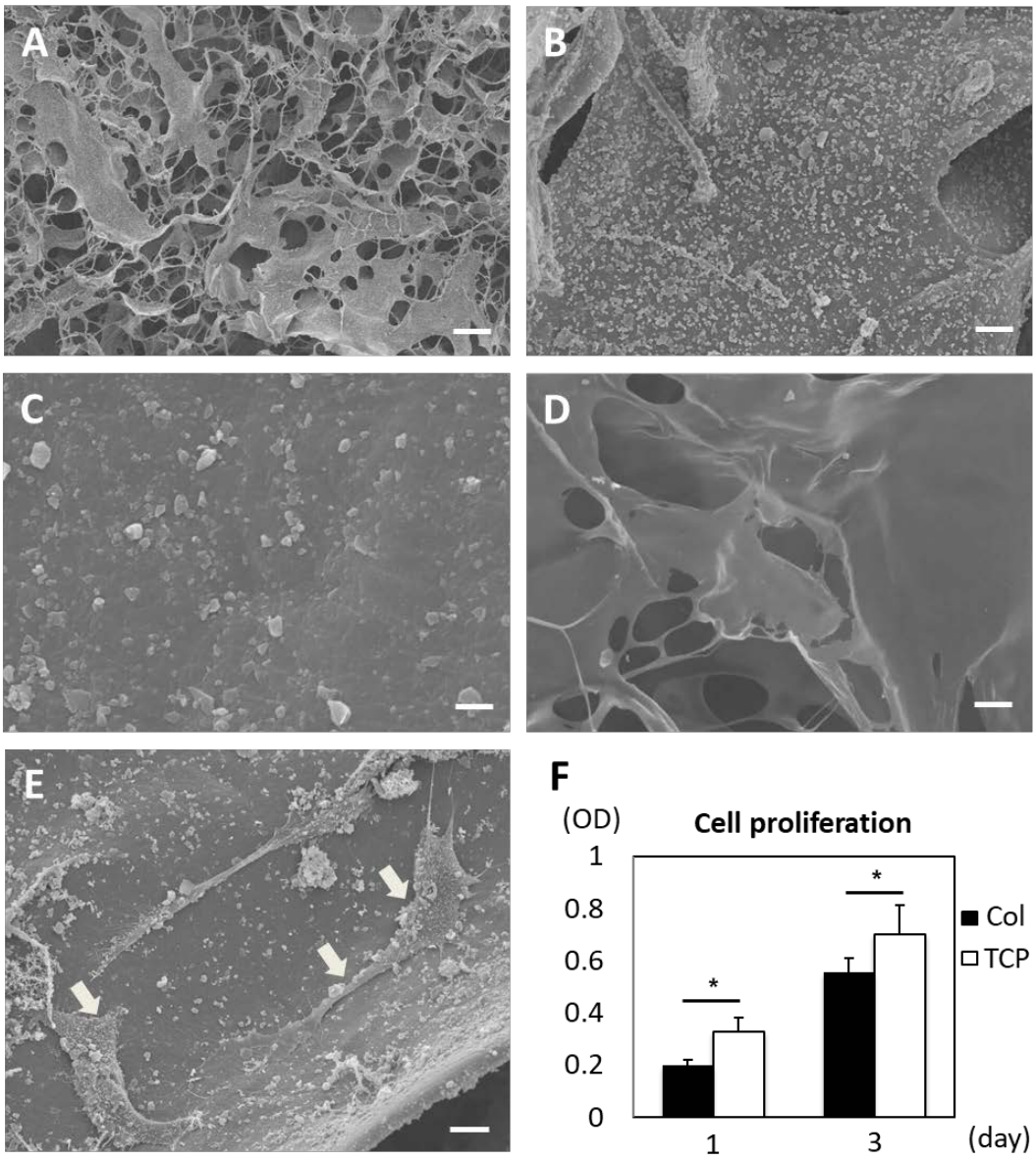

Figure 3

(A) SEM micrograph of nano-β-TCP scaffold. (B) Higher magnification of nano-β-TCP scaffold. Dispersal of β-TCP nanoparticles attached to the collagen scaffold surface. (C) Higher magnification of nano-β-TCP scaffold. TCP nanomorphology was acquired on the collagen surface. (D) SEM micrograph of the collagen scaffold. (E) SEM micrograph of MC3T3-E1 cells seeded on nano-β-TCP scaffold after 24 h of incubation. Cell spreading was observed on the nanomodified scaffold (arrows). Scale bars represent 100 μm (A), 10 μm (B, D, E), and 1 μm (C). (F) CCK-8 assays of MC3T3-E1 cell proliferation after 1 day and 3 days of incubation (N = 6, mean ± SD). Col and TCP respectively denote collagen scaffold and nano-β-TCP scaffold. *P < 0.05.

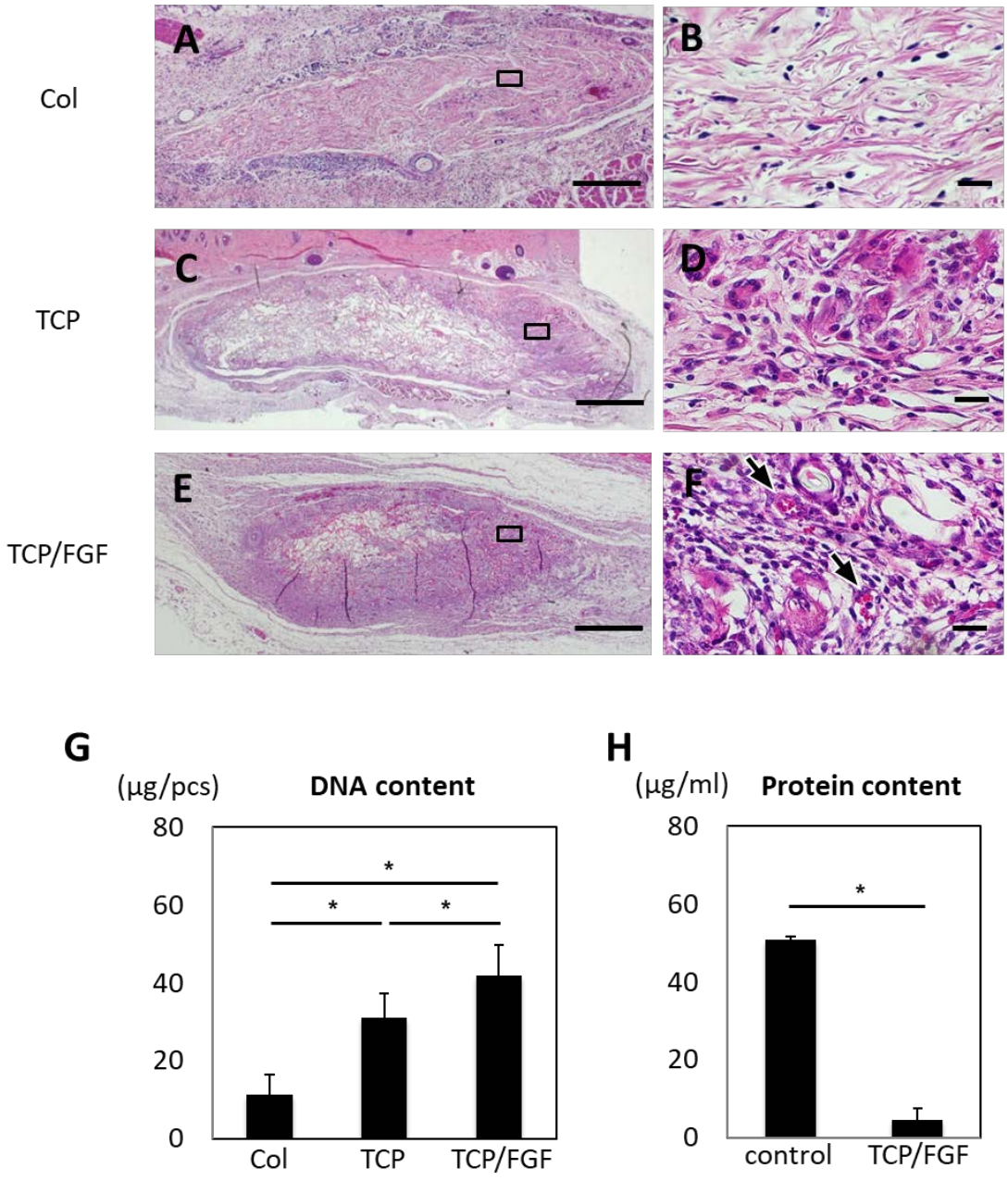

Figure 4

Histological findings from rat subcutaneous tests at 10 days. (A) Specimen implanted with collagen scaffold. (B) Higher magnification of framed area in (A). Cell and tissue ingrowth were rarely observed in the scaffold. (C) Specimen implanted with nano-β-TCP scaffold. (D) Higher magnification of the framed area in (C). Macrophage-like cells and fibroblastic cells were detected in the scaffold. (E) Specimen implanted with FGF-2-loaded nano-β-TCP scaffold. (F) Higher magnification of framed area in (E). Blood vessels (arrows), fibroblastic cells, and macrophage-like cells were observed frequently in the scaffold. Col, TCP and TCP/FGF respectively denote collagen scaffold, nano-β-TCP scaffold and FGF2 loaded nano-β-TCP

scaffold. Scale bars represent 1 mm (A, C, E) and 10 μm (B, D, F). Staining: hematoxylin and eosin. (G) DNA content of scaffolds implanted for 10 days in rats (N= 6, mean ± SD). Col, TCP, TCP/FGF, and pcs respectively denote collagen scaffold, nano-β-TCP scaffold, FGF-2-loaded nano-β-TCP scaffold, and pieces. * $P < 0.05$. (H) Protein assay of FGF-2 loaded scaffold (N= 4, mean ± SD). TCP/FGF indicate FGF-2-loaded nano-β-TCP scaffold. * $P < 0.05$.

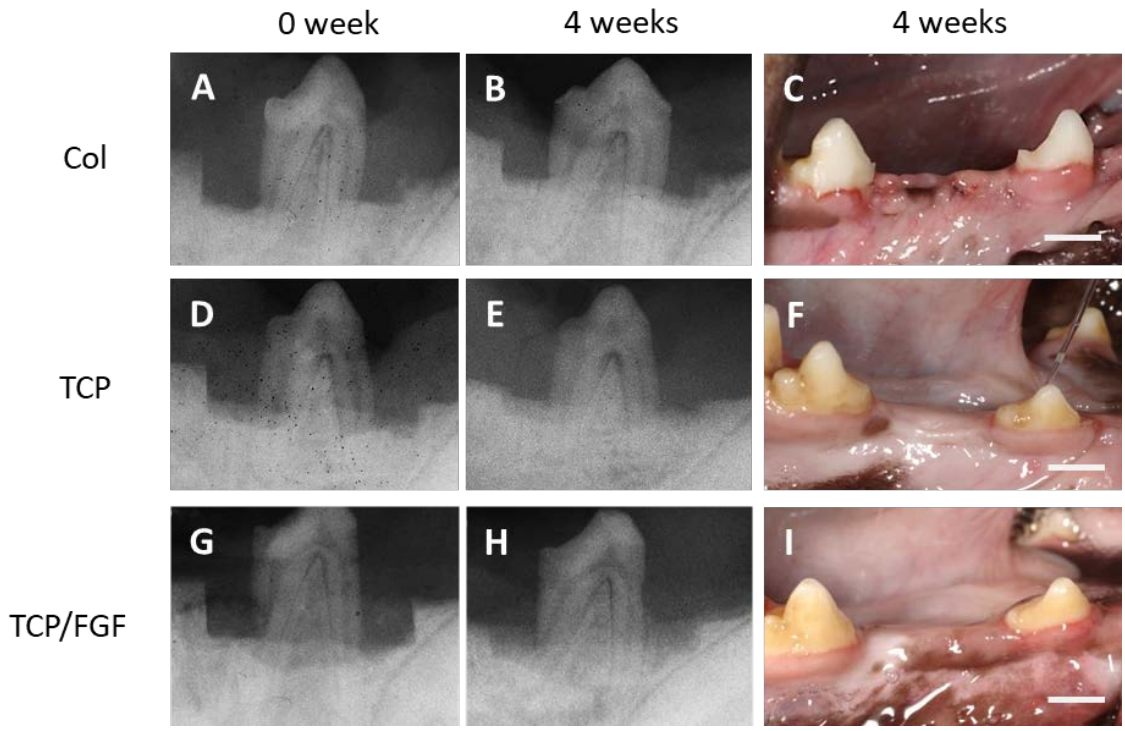

Figure 5

Radiographic images at 0 and 4 weeks, and macroscopic findings at 4 weeks post-surgery. (A), (B), (C) Images of collagen scaffold group. (D), (E), (F) Images of nano β-TCP scaffold group. (G), (H), (I) Images of FGF-2 loaded nano β-TCP scaffold. Col, TCP and TCP/FGF respectively denote collagen scaffold, nano-β-TCP scaffold and FGF2 loaded nano-β-TCP scaffold. Scale bars represent 5 mm.

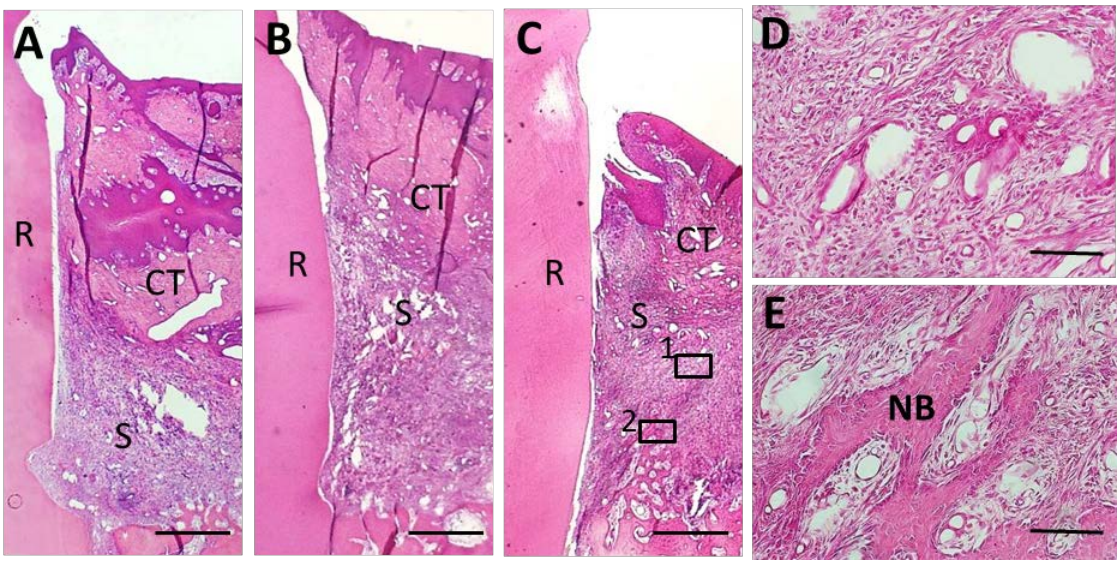

Figure 6

Histological findings of periodontal healing at 10 days. (A) Specimen receiving collagen scaffold. (B) Specimen receiving nano β-TCP scaffold. (C) Specimen receiving FGF2-loaded nano-β-TCP scaffold. (D) Higher magnification of framed area (1) in panel C. Ingrowth of blood-vessel-like tissue and fibroblastic cells were frequently observed. (E) Higher magnification of the framed area (2) in panel C. Woven bone formation was frequently promoted. Abbreviations: R, root; NB, new bone; CT, connective tissue; S, scaffold; Scale bars represent 1 mm (A, B, C) and 100 μm (D, E). Staining: hematoxylin and eosin.

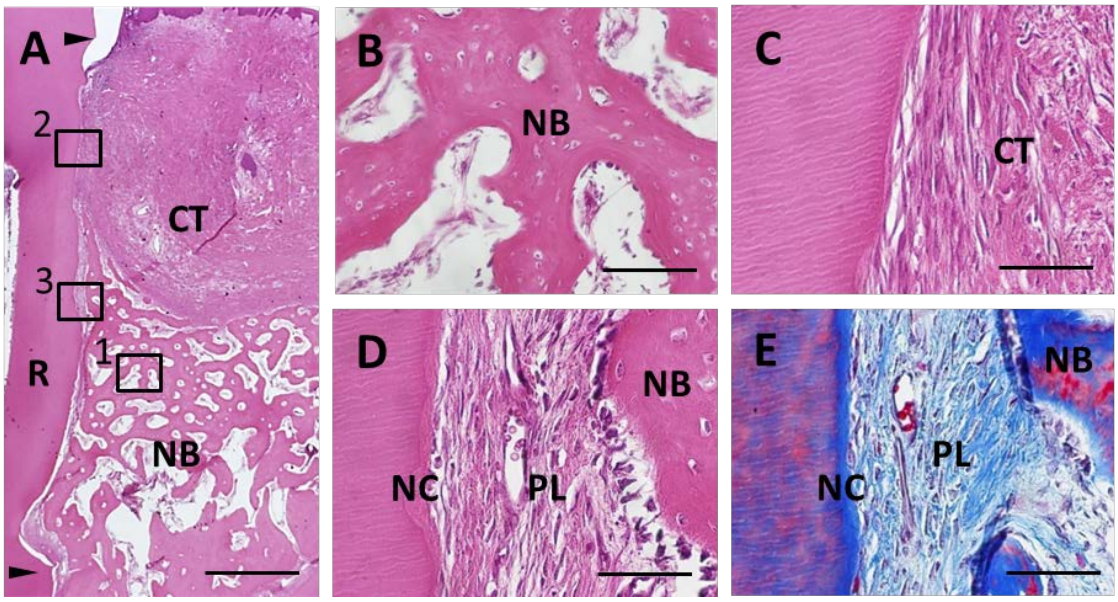

Figure 7

Histological findings of periodontal healing at 4 weeks. (A) Specimen receiving FGF2-loaded nano-β-TCP scaffold. Advanced periodontal tissue formation was observed. (B) Higher magnification of the framed area (1) in panel A. New bone containing osteoblast-like and osteocyte-like cells was generated. (C) Higher magnification of the framed area (2) in panel A. Connective tissue is attached to the root surface. (D) Higher magnification of the framed area (3) in panel A. Newly formed periodontal ligament-like tissue and cementum-like tissue were observed. (E) Newly formed fibrous tissue stained with Masson's trichrome. Arrowheads indicate reference notches. Abbreviations: R, root; NB, new bone; CT, connective tissue; NC, new cementum-like tissue; PL, periodontal ligament-like tissue; Scale bars represent 1 mm (A) and 100 μm (B, C, D, E). Staining: hematoxylin and eosin (A, B, C, D) and Masson's trichrome (E).

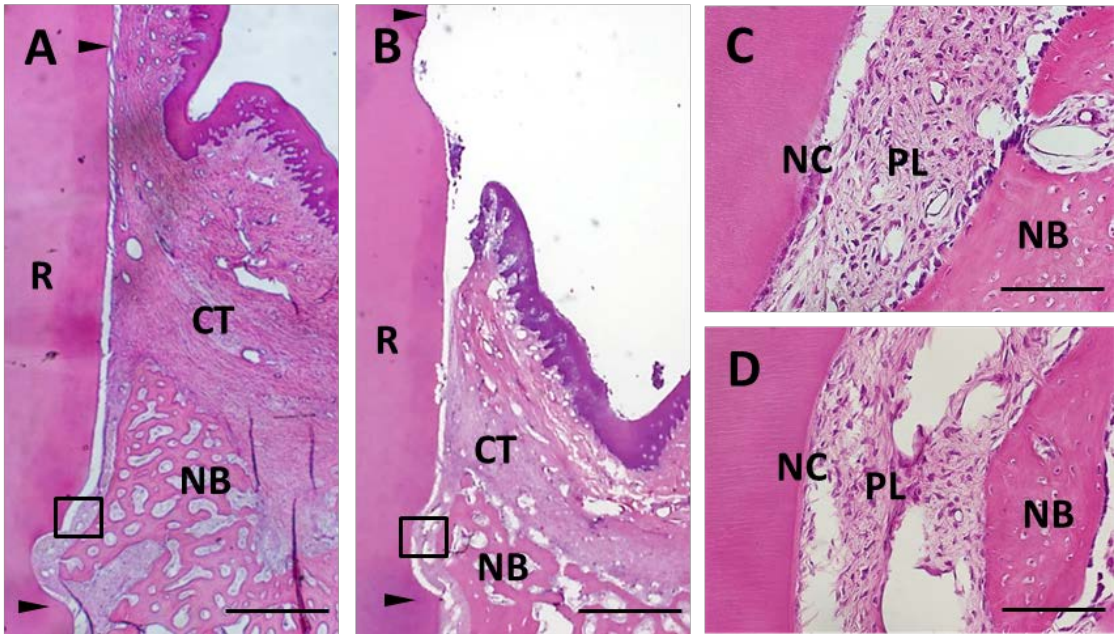

Figure 8

Histological findings for periodontal healing at 4 weeks. (A) Specimen implanted with nano β-TCP scaffold and (B) collagen scaffold. (C) Higher magnification of the framed area in (A). Periodontal ligament-like tissue was observed in the apical portion. (D) Higher magnification of framed area in (B). Periodontal ligament-like tissue was only rebuilt around the apical notch. Arrowheads indicate reference notches. Abbreviations: R, root; NB, new bone; CT, connective tissue; NC, new cementum-like tissue; PL, periodontal ligament-like tissue; Scale bars represent 1 mm (A, B) and 100 μm (C, D). Staining: hematoxylin and eosin.

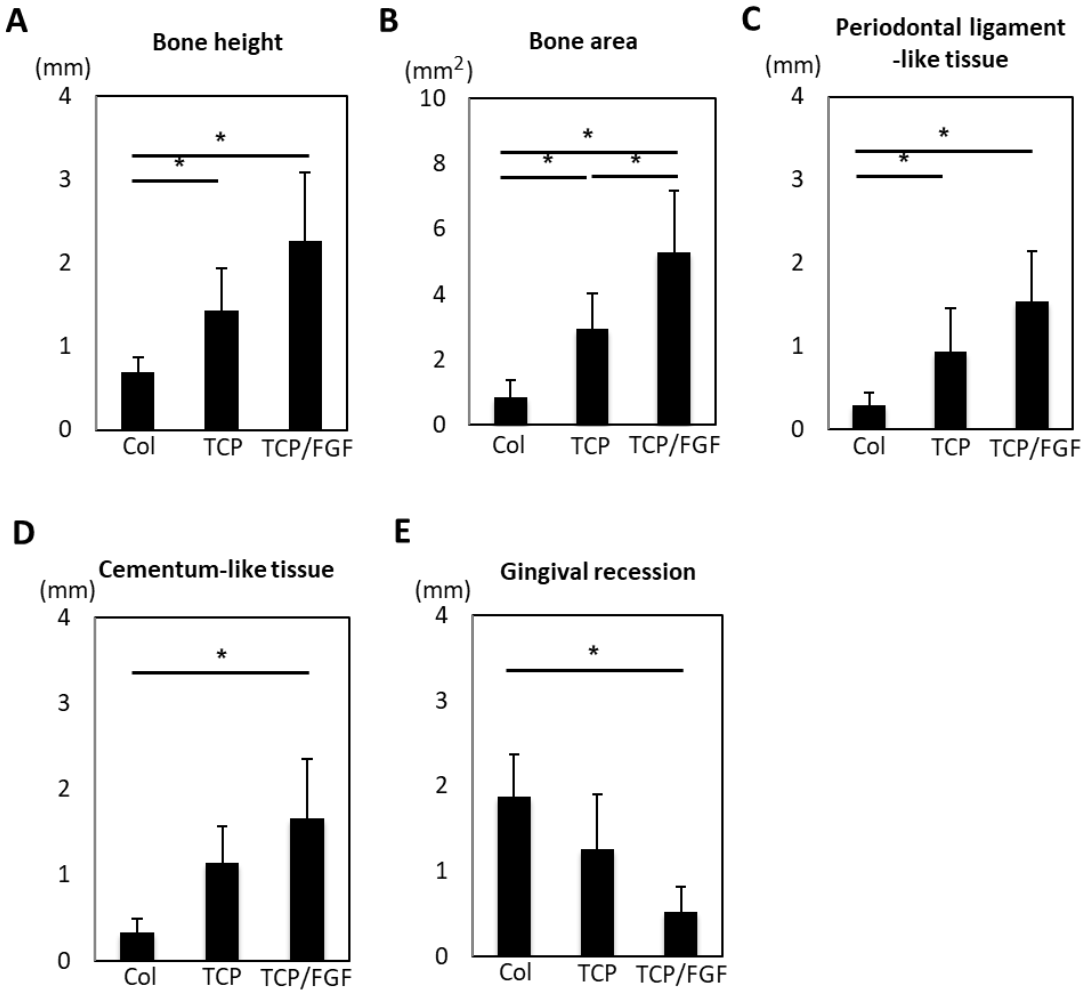

Figure 9

Histomorphometric analysis at 4 weeks (N = 7, mean ± SD): (A) bone height, (B) bone area, (C) periodontal ligament-like tissue, (D) cementum-like tissue, and (E) gingival recession. Col, TCP, and TCP/FGF respectively indicate collagen scaffold, nano-β-TCP scaffold, and FGF2 loaded nano-β-TCP scaffold. * $P < 0.05$.